

# Late MIS5a in the southern North Sea: new chronostratigraphic insights from the Brown Bank Formation

IRENE M. WAAJEN,<sup>1,2\*</sup> FREEK S. BUSSCHERS,<sup>2</sup> TIMME H. DONDERS,<sup>1</sup> SYTZE VAN HETEREN,<sup>2</sup> RUTH PLETS,<sup>3</sup> JAKOB WALLINGA,<sup>4</sup> RICK HENNEKAM,<sup>5</sup> GERT-JAN REICHART,<sup>1,5</sup> TIM KINNAIRD<sup>6</sup> and FRIEDERIKE WAGNER-CREMER<sup>1</sup>

<sup>1</sup>Faculty of Geosciences, Utrecht University, Utrecht, the Netherlands

<sup>2</sup>TNO – Geological Survey of the Netherlands, Utrecht, the Netherlands

<sup>3</sup>Flanders Marine Institute (VLIZ), Oostende, Belgium

<sup>4</sup>Soil Geography and Landscape group & Netherlands Centre for Luminescence dating, Wageningen University, Wageningen, the Netherlands

<sup>5</sup>Department of Ocean Systems, Royal Netherlands Institute for Sea Research (NIOZ), Den Burg, Texel, the Netherlands

<sup>6</sup>School of Earth and Environmental Sciences, University of St. Andrews, St. Andrews, UK

Received 28 June 2023; Revised 4 December 2023; Accepted 15 December 2023

**ABSTRACT:** The Brown Bank Formation (BB Fm) is a clay-rich sedimentary unit that is distributed over a large area in the southern North Sea. It is easily recognisable in 2D acoustic reflection profiles, forming sets of subparallel high-amplitude reflections. Previous studies have provided only fragmentary information on the facies, and a variety of interpretations on the depositional environment and age of the BB Fm. In this study we combine high-resolution 2D acoustic reflection profiles and multiproxy sedimentological, geochemical and geochronological analyses of three vibrocores, to provide a detailed description and a new age assessment for the BB Fm at its type locality, adjacent to the Brown Bank ridge. At the study site, the BB Fm shows morphologically well-preserved submarine sand dunes, deposited in a high-energy shelf setting, overlain by organic-rich silty clays that were deposited under lower-energy conditions in an increasingly compartmentalised marginal marine environment. Elevated terrestrial organic input shows that the Rhine–Meuse delta was situated relatively close-by. Luminescence ages indicate that the sediments of the BB Fm in our cores were deposited during the Weichselian Odderade interstadial (MIS5a, ca. 80 ka) and earliest parts of the Early Pleniglacial (MIS4, ca. 70 ka), which is later than previously reported in the literature.

© 2024 The Authors. *Journal of Quaternary Science* Published by John Wiley & Sons Ltd.

**KEYWORDS:** Early Weichselian; multi-proxy; chronostratigraphy; Brown Bank; North Sea

## Introduction

The Quaternary stratigraphic record of the southern North Sea consists of a stack of shallow-marine, coastal, fluvial and glacial sediments that were deposited under highly variable climate conditions, sea level oscillations and phases of glacial expansion and retreat. Of these sediment stacks, the Brown Bank Member (Dutch subdivision, TNO-GDN, 2023) or Brown Bank Formation (BB Fm, following the British subdivision) stands out as a distinct—but poorly constrained—unit in acoustic reflection data in the upper tens of metres of this record, with an even-parallel reflection configuration (Cameron et al., 1989; Laban, 1995; Missiaen et al., 2021; Oele, 1971). As most literature sources use the terminology ‘Formation’, this will be applied in this study.

Today the distinct layers of the BB Fm are used as an easily recognisable marker bed enabling correlation in the shallow subsurface of the southern North Sea, separating shallow marine Eemian sediments [Marine Isotope Stage (MIS)5e, ca. 130–115 ka] from typically terrestrial Weichselian (MIS4–2) and marine Holocene units (Fig. 1). Increasing relevance of the BB Fm comes from its presence within multiple windfarm sites, where it stands out in an overall sandy succession. Despite new borehole samples becoming increasingly available,

uncertainties remain on its geological age and depositional environment. These uncertainties inhibit confident age correlations and, consequently, broad-scale environmental reconstructions that are needed to understand the Late Pleistocene development of the southern North Sea basin.

The presently known distribution of the BB Fm in the southern North Sea stretches into large parts of the Southern Bight, with increasing patchiness toward its margins covering an area of more than 10 000 km<sup>2</sup> (Fig. 2A; Cameron et al., 1989). The average thickness of the BB Fm is 5 m; local maxima of up to 20 m tend to be limited to channel-fill-like features in some parts (Bicket & Tizzard, 2015; Cameron et al., 1992; Limpenny et al., 2011). In the past, the sediments were typically characterised as stiff, grey–brown laminated clays, showing local bioturbation (Cameron et al., 1992; Laban, 1995; Missiaen et al., 2021). Recently, the BB Fm has been subdivided into a relatively sandy Lower Brown Bank unit, with shell fragments, and a finer Upper Brown Bank unit, which consists mainly of clayey silt (Eaton et al., 2020; Wessex Archaeology, 2018). In 2D high-resolution acoustic reflection data, even finer subdivisions of the BB Fm are proposed (Missiaen et al., 2021 and references therein), indicating a more complex and heterogeneous depositional environment than previously thought.

Despite the considerable extent, thickness and recognisability of the BB Fm, a detailed description and consistent interpretation of its facies and depositional environments are still lacking. Initial interpretations marked the depositional setting of the BB Fm as freshwater-dominated on the basis of

\*Correspondence: Irene M. Waajen, as above.

E-mail: irene.waajen@tno.nl

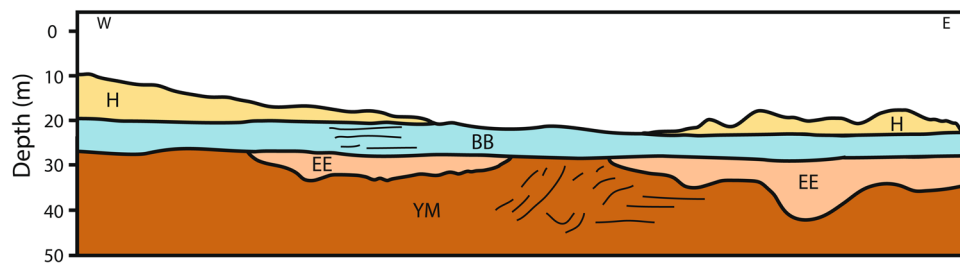


**Figure 1.** General profile of the shallow subsurface in the Brown Bank area, including ice-pushed structures in the Yarmouth Roads Formation (YR), Eemian marine sediments (EE), the Brown Bank Formation (BB) and Holocene superficial sediments (H). Based on Cameron et al. (1984). [Color figure can be viewed at [wileyonlinelibrary.com](http://wileyonlinelibrary.com)]

ostracod analysis (Oele, 1971; Zagwijn, 1983). The sedimentary facies of the BB Fm, studied in more than 100 vibrocores by Cameron et al. (1989), indicate a dominance of deposition in a shallow lagoon with restricted access to the open sea, based on the presence of the gastropod *Peringia ulvae* and in light of abundant evidence of bioturbation. These same authors reported that this saline or at least brackish succession is overlain by lacustrine deposits in the eastern part of the Brown Bank area. Vibrocores from the Norfolk Vanguard Offshore windfarm site contain marine to outer estuarine foraminiferal and ostracod assemblages in both the upper and lower BB Fm, indicating deposition in a transitional shallow-marine to lagoonal depositional setting (Eaton et al., 2020; Wessex Archaeology, 2018). On the basis of palaeo-environmental indicators, parts of it have been described as pro-delta plain deposits of the Rhine–Meuse river system (Hijma et al., 2012; Peeters et al., 2016). It is apparent that the BB Fm can be linked to a wide variety of depositional settings, but whether these different environments occurred side by side or in specific temporal successions remains to be tested.

Next to this remaining uncertainty on depositional conditions, the age of the BB Fm is also still poorly constrained, with a broad range from the late Eemian (late MIS5e, ca. 115 ka) to middle Pleniglacial (MIS3; ca. 50 ka). Initial indirect age estimates, based on pollen data, suggest deposition during the late Eemian to the early phase of the Early Weichselian (late MIS5e to MIS5d; ca. 115–100 ka) (Zagwijn, 1983). A small initial set of optically stimulated luminescence (OSL) analyses, compiled more recently, indicates that the age of the BB Fm ranges from 85 to 50 ka, corresponding to the period from the Odderade interstadial (MIS5a) to the Middle Pleniglacial (MIS3; Limpenny et al., 2011; Wessex Archaeology, 2018). This limited age constraint does not provide information on whether the unit was deposited throughout the entire period from the end of the Eemian to Middle Pleniglacial, or was restricted to specific shorter intervals within one or more stadials and/or interstadials. The lack of age control has hampered a refined determination of the depositional settings and their links to global sea level. However, the fact that the BB Fm represents Early Weichselian deposits may provide new insight into palaeo-environmental dynamics during the cooling phase of the last glacial cycle. As many studies focus on either warm periods such as the last interglacial, or warming periods such as the last deglaciation, the start of glaciation remains understudied. More insights into the interglacial–glacial transition can improve our understanding of the climate system under natural conditions (e.g. Sánchez Goñi et al., 2013). As a starting point, new chronostratigraphic constraints of sedimentary records from this time period are essential.

In this study we provide a thorough description and a new age assessment for the BB Fm from three vibrocores taken at its type locality close to the Brown Bank Ridge. We combine high-resolution 2D acoustic reflection profiles and sediment analyses, integrating detailed records of organic matter content, elemental

composition and luminescence ages accompanied by pollen biostratigraphy. This multiproxy analysis provides a new framework on the depositional environment of the BB Fm at this location, facilitating the systematic sedimentological interpretation of a regional acoustic marker bed. In a parallel study, these sediment characteristics are used to further characterise the palaeo-environment of this part of the southern North Sea during the period of deposition.

## Physical setting

The study site is located in the Southern Bight of the southern North Sea, 83 km offshore the Dutch coast, in an area where Late Pleistocene deposits of the BB Fm are almost omnipresent (Fig. 2A) (e.g. Cameron et al., 1989; Missiaen et al., 2021; Oele, 1971; Zagwijn, 1983). The BB Fm is named after the largest tidal sand ridge in the southern North Sea: the Brown Bank ridge (Fig. 2B). A narrow and elongated trench, named ‘Het Gat’ by fishermen, is located east of this ridge. Het Gat forms the deepest part of a large area of tidal ridges and swales that dominate this part of the North Sea, and is well known for its early Pleistocene vertebrate fauna (Mol et al., 2003). The core site (Fig. 2C) is situated on the eastern flank of Het Gat (hereafter abbreviated FG), which has also been described in Missiaen et al. (2021) (VC34–VC37). The current water depth at the location is 39 m below mean sea level (MSL).

## Methods

### Geophysical survey

2D high-resolution acoustic reflection profiles were collected in a grid over Het Gat (Fig. 2B) using a multi-transducer parametric echosounder (MPES) onboard the Belgian Research Vessel RV *Belgica* in 2018 (N–S line Fig. 3) and in May 2019 (W–E line Fig. 3) (also described by Missiaen et al., 2021). This parametric system was pole-mounted and the four transducers were arranged in a square single-beam set-up with a secondary low frequency of 6 kHz, providing decimetre-scale resolution up to 15 m penetration depth. Additional processing, performed in RadExPro, consisted of amplitude balancing, filtering (burst noise removal and 2D spatial filtering) and tidal corrections (lowest astronomical tide). A velocity of 1550 m s<sup>-1</sup> was used for depth conversion.

### Sediment cores

The coring locations were selected on the basis of the 2018 MPES results. To ensure that each vibrocore would fully penetrate the BB Fm and reach the underlying sediments, the base of the even, parallel reflections typical of the BB Fm had to be located within 3 m below seafloor. Three vibrocores, within 40 m of each other

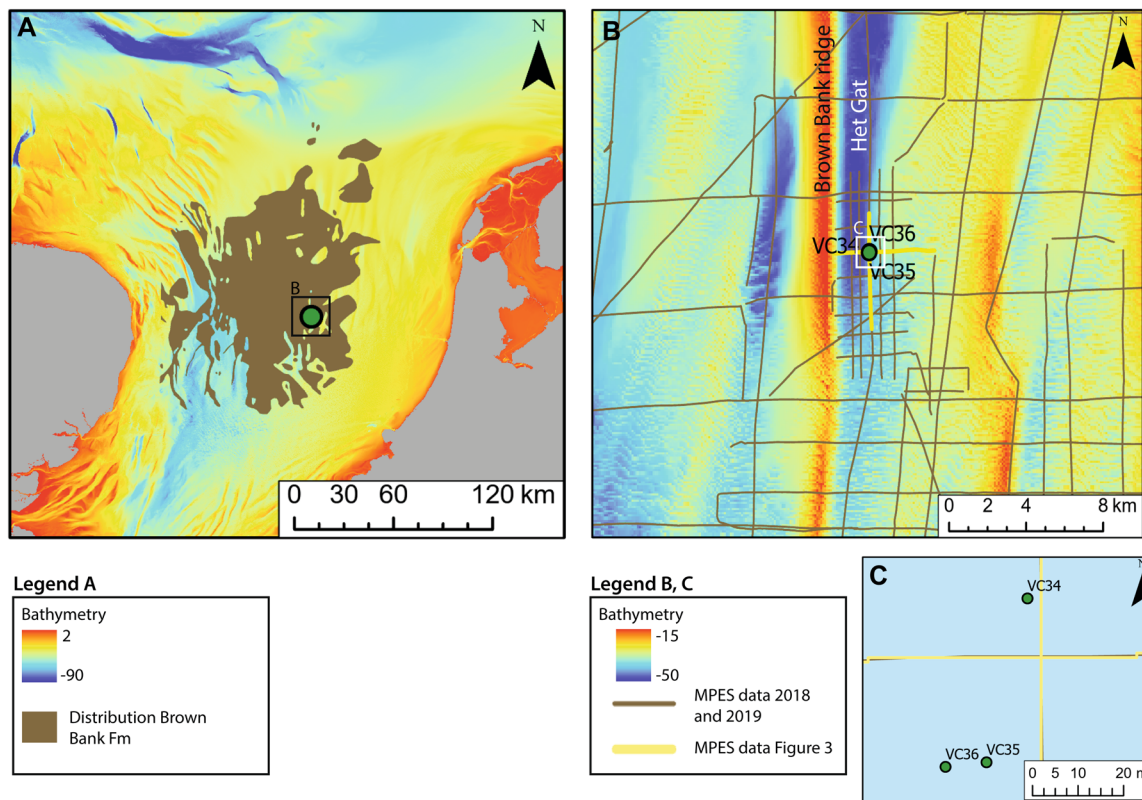


**Figure 2.** Geographical setting of the study site in the southern North Sea. (A) Bathymetric map of the southern North Sea (EMODnet Bathymetry Consortium, 2020), including the distribution map of the Brown Bank Fm (Cameron et al., 1989) indicating the main presence of the BB Fm, although new data suggest a slightly more extensive distribution. (B) Insert of the bathymetric map surrounding the Brown Bank tidal ridge and Het Gat, including the grid of MPES data retrieved in 2018 and 2019. The yellow lines denote the acoustic profiles shown in Fig. 3. (C) Inset of the location of the three cores. [Color figure can be viewed at wileyonlinelibrary.com]

(Table 1), were taken onboard RV *Pelagia* (cruise 64PE439) in July 2018 using a Marine Sampling Holland electrical vibrocorer with a maximum penetration of 5 m. Water depth was determined relative to MSL based on a multibeam echosounder on board RV *Pelagia* and corrected for tidal fluctuations.

Core VC34 was split under red light conditions at the University at Warwick, with one half transferred to the University of Wales Trinity Saint David, Lampeter campus, for sedimentological descriptions and photographed as part of the Europe's Lost Frontiers project. Cores VC35 and VC36 were stored at the Geological Survey of the Netherlands (GSN) and were split in a dark room before photographs and sedimentary logs were made. The core descriptions of the three cores can be obtained at the DINOloket database using the GSN numbers in Table 1.

### Loss on ignition (VC35, VC36)

Loss on ignition (LOI) was measured on samples from cores VC35 and VC36 to study the organic matter content (mass percentage), and used to correlate the two cores. For LOI, the

**Table 1.** Location data on the three vibrocores used in this study.

Core no.	Coordinates (WGS84-UTM31N)	Penetration (cm)	Water depth (m MSL)	Number GSN
VC34	523775, 5827987	266	39.28	BP080111
VC35	523766, 5827951	300	39.83	BP080094
VC36	523757, 5827950	305	39.78	BP080095

core surface was cleaned and sediment samples of  $\sim 1 \text{ cm}^3$  were taken at 1-cm vertical resolution. The samples were dried in a stove at  $105^\circ\text{C}$  and combusted at  $550^\circ\text{C}$ . LOI was calculated as:

$$LOI = \frac{DW_{105} - DW_{550}}{DW_{105}} * 100\%$$

with  $DW_{105}$  denoting bulk dry weight and  $DW_{550}$  the weight of the mineral content (Bos et al., 2012; Dean, 1974; Heiri et al., 2001).

### Luminescence dating (VC34, VC35, VC36)

Luminescence dating determines the timing of last light exposure of quartz or feldspar minerals, and thus the time of deposition and burial of sediments. For our study, luminescence analyses were independently conducted at two laboratories: samples from VC35 and VC36 at the Netherlands Centre of Luminescence dating (NCL) and samples from VC34 at the luminescence laboratories at the School of Earth Environmental Sciences (SEES), University of St Andrews. NCL's investigations were performed on both sand-sized feldspar, measuring single-grain K-rich feldspar post-infrared infrared-stimulated luminescence (pIRIR; e.g. Reimann et al., 2012), and sand-sized quartz OSL (e.g. Murray et al., 2021). SEES's investigations of core VC34 focused on quartz OSL only. Four samples from sand-rich intervals were taken from cores VC35 and VC36, where an  $\sim 10$ - to 15-cm vertical interval was obtained from the split core in safe light conditions at GSN, and further prepared and analysed at NCL. Core VC34 was split under red light conditions at the University at Warwick. Eight samples were analysed for OSL at SEES (see Fig. 4 and Table 2 for sample depths).

OSL and pIRIR protocols are used to quantify the ionising radiation dose absorbed since the last light exposure of quartz and feldspar mineral grains, respectively. A burial age is obtained by dividing this palaeodose by the annual ionising radiation dose absorbed by the minerals (dose rate). All luminescence measurements were performed on sand-sized grains, and a range of checks was performed to test the suitability of the adopted protocols. Luminescence dating methods are continuously in development and not fully standardised between labs. The NCL and SEES facilities operated independently during this project and used different techniques for estimating the effective environmental dose rate and slightly different approaches for measurement and analysis of luminescence signals. Given that three different protocols were used, providing all details in the main text would hamper readability. A full account of measurement details, dose–response curves and age distributions is provided in Supporting Information S.1 (NCL) and S.2 (SEES).

One of the main challenges in luminescence dating of these samples was saturation of the quartz OSL signal. When the OSL signal approaches saturation, accurate dating is no longer possible. The threshold of  $2D_0$  (e.g., Wintle & Murray, 2006) is often used to assess the validity of results, where the  $D_0$  parameter quantifies the ‘onset of saturation’ and equivalent doses ( $D_e$ ) above  $2D_0$  are regarded as unreliable. At SEES, single-aliquot  $D_e$  results above the saturation threshold were rejected, and the central dose model (Galbraith et al., 1999) was applied to the remaining data. The dates become less reliable with higher percentages of aliquots above  $2D_0$ . If more than 35% of the single-aliquot data was above the saturation threshold, the result is interpreted as a minimum estimate of the palaeodose. If fewer data were rejected, the result is regarded as a reliable estimate of palaeodose. Measurements were made on two different grain size fractions, and differences in effective environmental dose rates to these fractions were taken into account. At NCL, single-aliquot  $D_e$  values above the saturation threshold were included in the palaeodose estimation. For samples where more than 35% of single-aliquot data was above  $2D_0$ , results are less reliable and presented as ‘best-estimate’ ages. In addition, feldspar pIRIR analyses were performed to obtain burial ages for samples where the OSL was close to saturation. The pIRIR signals saturate at greater doses, and thus may be used to date older samples (e.g. Wallinga & Cunningham, 2015). The pIRIR measurements were performed on single grains to detect potential heterogeneous bleaching. Results obtained using this method are less robust than unsaturated quartz ages, due to uncertainties related to poor dose recovery and anomalous fading (see S.1 for detailed information and discussion). Exact comparison of the ages obtained by the two facilities is not possible due to the different approaches used, but the combined information from all luminescence analyses provides a sufficiently robust chronological framework to interpret the depositional age of the Brown Bank deposits.

### Palynology (VC35)

Pollen analyses were used to identify stratigraphically relevant assemblages as defined in previously described pollen zones. Indirect age constraints provided by this method complement the OSL dating results; their comparison provides a first-order indication of consistency and, possibly, reliability. Pollen analyses were performed on 24 samples of  $0.67\text{ cm}^3$ , taken at 12-cm vertical intervals. Carbonates were removed by 5% HCl, after which humic material was removed by 5% KOH treatment for 60 min at  $70\text{ }^\circ\text{C}$  and by sieving of the residue over a coarse ( $120\text{ }\mu\text{m}$ ) and fine ( $6\text{ }\mu\text{m}$ ) mesh. Most organic debris

was dissolved by 5 min of acetolysis at  $100\text{ }^\circ\text{C}$  (acetic anhydride and sulphuric acid, 9:1 v/v). Finally, the remaining organic material was separated from siliciclastic material by heavy liquid flotation over sodium polytungstate with a density of  $2.0\text{ g cm}^{-3}$ . Samples were mounted on glass slides in glycerol. For each sample at least 200 pollen grains were counted. Freshwater algae *Pediastrum* and *Botryococcus* were also counted, as well as dinoflagellates and foraminifera linings. The pollen sum used for this study includes all tree, shrub, heath and herb pollen and excludes Cyperaceae, spores, and aquatic pollen.

### X-ray fluorescence core scanning (VC35, VC36)

X-ray fluorescence (XRF) core scanning was used to document the bulk geochemical characteristics of cores VC35 and VC36. XRF core scanning was performed with an Avaatech scanner at the Royal Netherlands Institute for Sea Research (NIOZ). Prior to scanning, the cores were covered with a  $4\text{-}\mu\text{m}$  SPEXCerti Ultralene foil, to avoid contamination of the measurement prism by the sediment. Vertical measurement step size was 10 mm using a slit size of 10 mm down core and 12 mm cross core. Elements were measured at three energy settings (10 kV, 0.5 mA, 15 s; 30 kV, 0.25 mA, 15 s; and 50 kV, 1.5 mA, 30 s). Core VC36 was measured from the top down to 281 cm depth. Below this level, the irregular cutting surface made further measurement impossible. VC35 was measured from its top down to 279 cm depth. Gaps in the record represent depth intervals sampled for OSL dating, and one interval where the core was too irregular to be measured. The element intensities (counts per second; cps) acquired by the XRF core scanner will be presented as logarithmic ratios between element (Aitchison, 1982), as is standard practice for XRF core scanning (e.g. Weltje & Tjallingii, 2008), or if individual elements are shown, after centred log-ratio transformation (clr; e.g. Martin-Puertas et al., 2017).

## Results

### Stratigraphy and lithology

At the core location, the grid of sub-bottom data shows a N–S-oriented depression (black line in Fig. 3) where the sedimentary infill is truncated by Het Gat, the present-day trench east of the Brown Bank ridge. The lowest unit in the acoustic reflection profiles (YR in Fig. 3B, D) is not reached by the sediment cores and probably belongs to the middle to lower Pleistocene Yarmouth Roads Fm, consisting of complex delta-top deposits (Cameron et al., 1992). The top of this unit resembles a hiatus and is covered by an acoustic transparent (sandy) unit having a dune-shaped morphology (SD), of which the top is present in the sediment cores. Above SD lies the Brown Bank unit with parallel reflection configurations, consisting of a dense acoustic facies at Het Gat (BB1), representing the depression infill, and a more transparent facies in the stratigraphic shallower parts (BB2). Unit BB2 is only present east of Het Gat and seems to be eroded at Het Gat. The top of the Brown Bank represents an erosional surface (green line in Fig. 3), overlain by younger sediments (Y) east of Het Gat. The N–S profile (Fig. 3C, D) shows how unit BB1 drapes over well-preserved submarine sand dunes (SD). The exceptional preservation of the buried dune topography is remarkable and may suggest that no major hiatus exists between the final phase of sand-dune formation and the initiation of BB Fm deposition at this location. BB2 seems absent in the core location, but might be present as a thin interval towards the top.

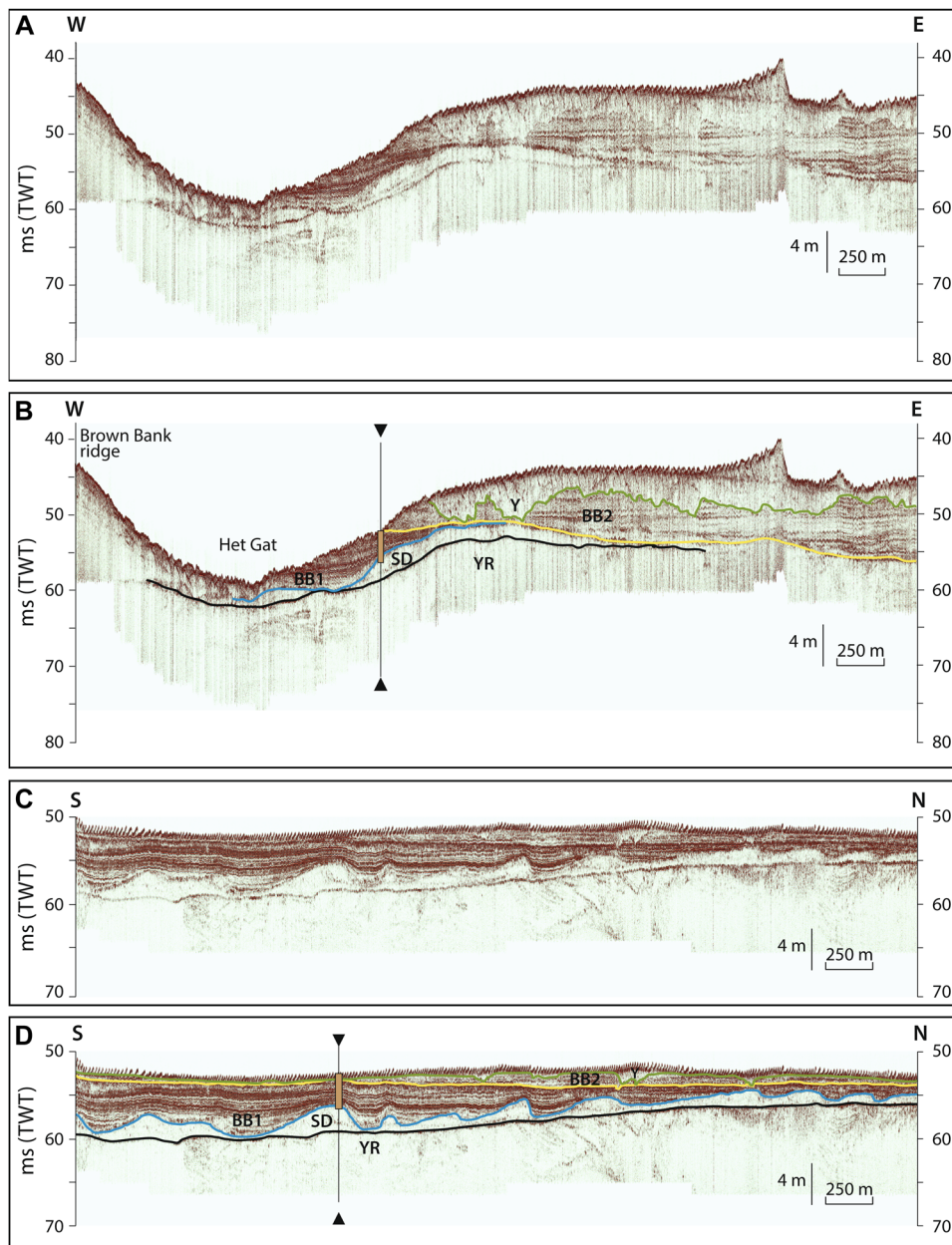


**Figure 3.** 2D high-resolution acoustic profiles along the core locations, with the brown vertical bar representing the cluster of the three vibrocores. (A) W–E acoustic profile. (B) Interpreted W–E acoustic profile including annotations and the locations of the Brown Bank Ridge, Het Gat and the core location FG. (C) N–S acoustic profile along Het Gat, with fully preserved sand dunes beneath the BB Fm. (D) Interpreted N–S acoustic profile including annotations. YR = deposits of the Yarmouth Roads Fm, SD = sand dune unit, BB1 = dense Brown Bank facies, BB2 = more transparent BB facies, Y = younger sediments. The line with triangles represents the crossing line of the other profile. [Color figure can be viewed at [wileyonlinelibrary.com](http://wileyonlinelibrary.com)]

The investigated cores show a succession of three distinct lithological units (Fig. 4). Sand at the base can be correlated with the sand dunes discerned on the sub-bottom data (SD, Fig. 3). This poorly sorted, medium rounded fine sand was black when the cores were opened, but oxidised to orange over time. The top of this sand, between 250 and 270 cm below seafloor, is overlain by the clay- and silt-rich BB Fm. This unit contains sand laminations and sand lenses varying in thickness between 1 mm and 2 cm. There are intervals of mainly clayey silt and silty clay, with sandy layers and lenses, as well as sandy and loam intervals with clay and silt layers and inclusions. Small inclusions of different grain size from the matrix, representing small-scale bioturbation, are present at multiple intervals throughout the clay-rich unit. However, preserved layers indicate that the stratigraphic succession has not been fully mixed, corroborating the intact subparallel reflection configuration of the BB Fm in 2D

acoustic reflection profiles. At around 45 cm below seafloor, a 1-cm-thick shell-rich, coarse sand and gravel layer is present. It is unclear if this layer represents the boundary between BB1 and BB2, as no sedimentological differences are visible above and below this coarse layer. The top unit of the cores, 12–23 cm thick, consists of a yellow-brown sand layer, interpreted to be the Holocene Southern Bight Formation (H). This sand is poorly sorted, medium rounded fine sand, similar to the sand from the sand dunes. In the top 60 cm of the clay-rich BB, some sand from the top Southern Bight layer is present in burrows.

### LOI

The organic content throughout cores VC35 and VC36 is below 10% (except for one outlier at 184 cm depth in core VC36) with an average of 3.7% (Fig. 4). In general, the organic

content is higher in clay-rich intervals than in sandy intervals. Both analysed cores show highly similar variability in organic content, which was used for correlation. The main difference between the cores occurs between 200 and 230 cm depth, where an interval of sandy clay with lower organic content is present in VC36, contrasting with an interval of mainly clay with higher organic content in VC35. As the sand dune unit starts higher in VC35 than in VC36, the part deeper than 200 cm may be more complete in VC36.

### Luminescence dating

Due to challenges with quartz OSL signal saturation [see 'Luminescence dating (VC34, VC35, VC36)', and Supporting Information S1 and S2], robust burial ages could only be obtained for the sand dune deposits below the BB-clay deposits. These deposits were within the reliable quartz OSL dating range owing to much lower effective environmental dose rates compared to the overlying clayey deposits of the BB unit. The quartz OSL ages from the sand dune unit yield an average age of  $89 \pm 5$  ka (Fig. 4 and Table 2). This age indicates deposition during the end of the Heringstadial (MIS5b) or during the Odderade interstadial (MIS5a). The feldspar pIRIR age from the sand dune (VC35-3F) is 20 ka younger than the quartz results. Together with the low dose recovery ratio obtained for feldspar, this may point to an underestimation of the ages obtained through feldspar pIRIR dating.

Reliability of luminescence ages obtained on the BB clay deposits is low due to quartz OSL signal saturation, and questionable performance of the feldspar pIRIR dating protocol used. Nevertheless, the quartz OSL minimum ages (SEES), best-estimate ages (NCL), feldspar pIRIR results and robust OSL ages on the underlying sand dune deposits provide a useful chronological framework. For VC34, quartz OSL minimum ages range from  $65 \pm 4$  ka for the topmost sample to  $82 \pm 10$  ka for the bottom sample. Sample VC34-2 Q is regarded as an outlier due to potential light contamination during sampling. For VC35, quartz OSL best-estimate ages yield estimates of  $69 \pm 5$  and  $70 \pm 5$  ka, while for VC36 an age of  $83 \pm 5$  ka was obtained for the same interval. Feldspar pIRIR ages are similar to the quartz OSL best-estimate ages, and range from  $56 \pm 5$  to  $76 \pm 6$  ka. The youngest result of  $56 \pm 5$  ka causes an age reversal, and is much younger compared with the quartz results from the same sample, pointing towards an underestimation of feldspar pIRIR ages and is therefore excluded from further age interpretation. The quartz OSL best-estimate ages combined with feldspar ages for VC35 and VC36 yield an average age of  $73 \pm 5$  ka. Quartz OSL minimum ages from VC34 as well as the quartz OSL ages on the underlying sand-dune deposits are consistent with this age estimate. We note, however, that the samples with lowest percentage of  $D_e$  estimates in saturation (39 and 40%  $>2D_0$ ; samples VC34-6, VC35-2Q and VC36-1Q) return the greatest ages, of which the ages obtained on VC34-6 and VC36-1 suggest that the BB-clay deposition started before 80 ka, and thus that the average age of  $73 \pm 5$  ka might be underestimated. The average age of the BB clay unit suggests deposition between 80 and 70 ka, ranging from the Odderade interstadial (MIS5a) into the Early Pleniglacial (MIS4).

Several lines of evidence suggest that the results are not affected by poor bleaching.  $D_e$  distributions of individual samples showed overdispersion of 15–40% (SEES) and 24–45% (NCL), which is typical for small-aliquot data in this dose range. Overdispersion of feldspar single grain  $D_e$  distributions is similar for all samples (34–44%), and also in line with what is expected for well-bleached samples in this

dose range. Moreover, in case of poor bleaching feldspar pIRIR ages would be expected to be greater than quartz OSL signals as they are less easily bleached (e.g. Murray et al., 2012), but this is not the case.

### Palynology

In the BB clay unit, about 80% of all pollen grains have been identified as tree pollen, indicating a forested environment (Fig. 5). *Pinus* is the most abundant pollen type, averaging around 50%. Furthermore, pollen of deciduous trees, including some thermophilous trees such as *Quercus*, *Corylus* and *Carpinus*, are present. Besides trees, grasses (*Poaceae*) and sedges (*Cyperaceae*) are also abundant. *Chenopodiaceae* is present in most samples, and might indicate a nearby coastal environment. The sand dune unit is almost barren in pollen, accompanied by a poorer preservation, resulting in unreliable low pollen counts (50–60 pollen per sample), making the results less reliable compared to the BB clay unit. The sand dune unit contains more monolet spores, and 60–70% of all pollen is tree pollen. This is slightly less than in the BB clay unit, but these differences have to be treated with caution due to the low pollen counts. There is little succession in the pollen assemblage. The pollen analyses indicate deposition in a cool-temperate climate.

The presence of marine dinoflagellates (*Spiniferites*, *Operculodinium*) indicates a marine depositional setting. The continuous presence of *Pediastrum*, a freshwater algae, indicates a constant inflow of fresh water. As the depositional setting during all sedimentary units is not terrestrial, all pollen must have been transported to this site, and therefore these pollen represent the vegetation of the regions surrounding the North Sea during deposition.

### XRF core scanning

The geochemical composition in the cores is dominated by the relative contribution of sands, clays, carbonates and organic matter. The  $\log(\text{Si}/\text{Al})$  ratio is used to determine the relative proportion of quartz sand (rich in Si) and clays (rich in Al) in the sediment (Van Hoang et al., 2010). High values of  $\log(\text{Si}/\text{Al})$  indicate sandy intervals, while low values are associated with clay-rich intervals (Fig. 6). The trends in  $\log(\text{Si}/\text{Al})$  strongly resemble the observed variations in grain size. The variations are highly similar in cores VC35 and VC36, after applying a vertical offset of ~5 cm to line up the top of the BB unit in both cores (Fig. 6C). This provides independent confirmation that the correlation based on LOI-derived organic carbon content is correct, and thus that the sedimentological succession is uniform over a distance of at least 10 m, as was expected from the subsurface data.  $\log(\text{Si}/\text{Al})$  correlates negatively to the LOI data in both cores (Fig. 6A, B), with high organic matter content in clay-rich intervals (low Si/Al) and lower amounts in sandier intervals, especially in units H and SD (high Si/Al). Below 215 cm depth, the similarity between the cores decreases, comparable to observations in LOI trends.

The geochemical variability associated with clay mineral input is well represented, for example by Al, K, Ti, and Fe. By taking a ratio to Ca, this also incorporates the relative contribution to carbonates.  $\log(\text{Ti}/\text{Ca})$ ,  $\log(\text{Al}/\text{Ca})$ , and K and Fe (clr) provide indicators for terrigenous input (e.g. Blanchet et al., 2009; Carlson et al., 2008; Harff et al., 2011; Tjallingii et al., 2010) and show comparable variations throughout the BB clay unit (Fig. 6). The terrigenous clay content varies throughout the BB clay unit, which could represent variations in sedimentation rates or a variable input of material to the site through time. The Holocene sand unit has relatively low Fe

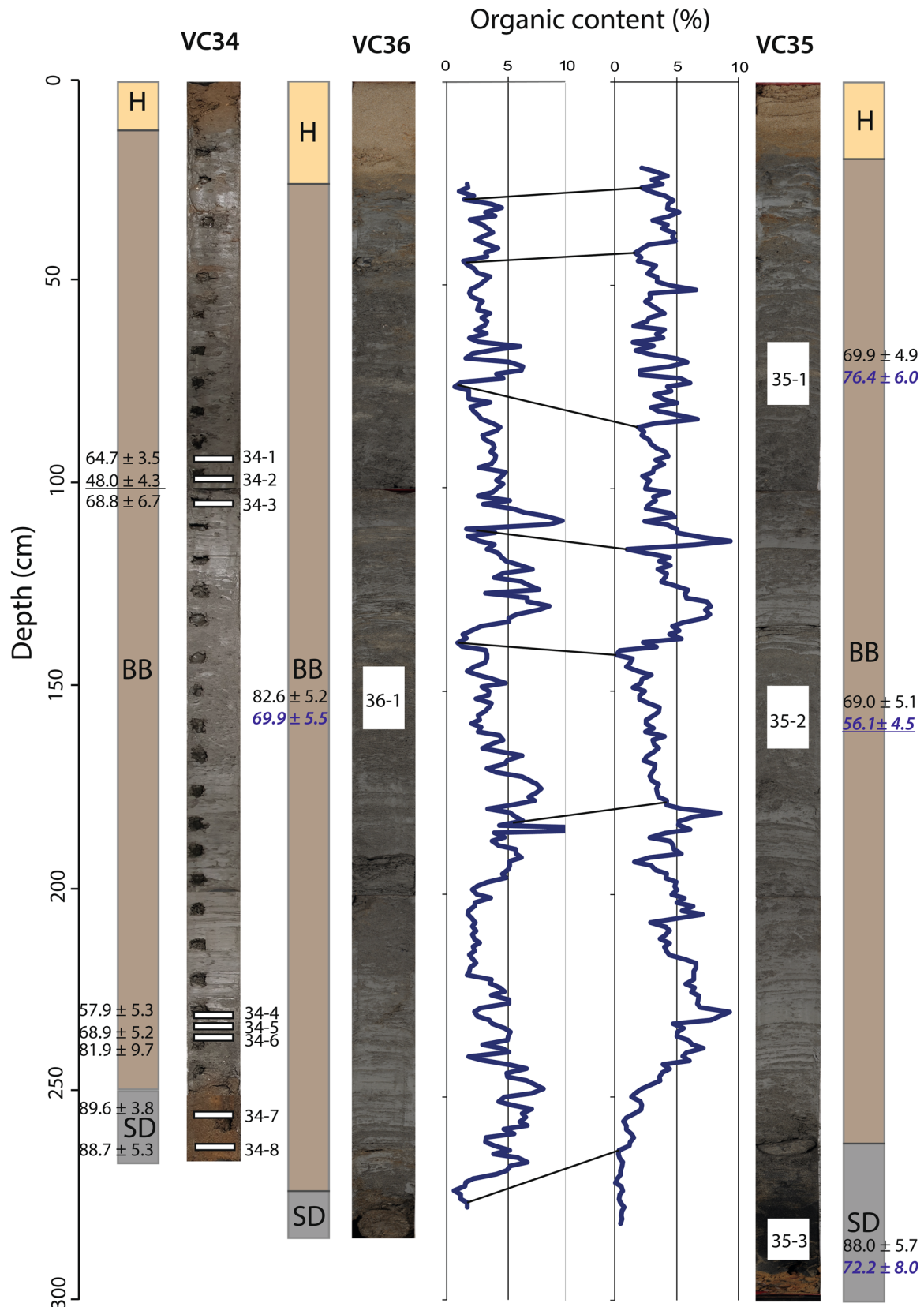


**Figure 4.** Core photographs showing the three different units: H = Holocene Southern Bight Formation, BB = Brown Bank clay-rich unit, SD = sand dune unit. Organic matter content from LOI measurements is used to correlate VC35 and VC36. The dashed line is based on the top of the sand dune unit and does not imply correlation of the overlying BB Fm. The depth intervals of luminescence samples are indicated by white rectangles. Quartz OSL ages are provided in black, feldspar pIRIR results in italic blue. The unreliable ages of VC34-2 and VC35-2 are underlined. [Color figure can be viewed at [wileyonlinelibrary.com](http://wileyonlinelibrary.com)]

content, while the sand dunes have relatively low K content, indicating that these two sand units have different geochemical signatures. Both carbonates (Ca) and clays are probably reduced within these sands which is likely to be related to

lower carbonate preservation, resulting in an increase in  $\log(\text{Ti}/\text{Ca})$  and  $\log(\text{Al}/\text{Ca})$ . In both sand units the variation in terrigenous elements is smaller, probably relating to constant input of sand.

**Table 2.** Luminescence dates of single-aliquot quartz (Q) OSL and single-grain feldspar pIRIR dating (F, in italics). Further details are provided in the Supporting Information. Feldspar ages were corrected for anomalous fading following Huntley and Lamothe (2001). The samples were measured with different techniques by the two different laboratories (<sup>1</sup>SEES, St. Andrews in 2021; <sup>2</sup>NCL Wageningen in 2023). For VC34 palaeodoses are provided for both the 150–250  $\mu\text{m}^a$  and 90–150  $\mu\text{m}^b$  fractions. Samples from the sand dune unit have orange rows, and from the BB clay unit have blue rows.

Sample	Lab code	Depth (cm)	Palaeodose (Gy)	Effective environmental dose rate (Gyka <sup>-1</sup> )	Age (ka)	Comments
VC34-1 Q <sup>1</sup>	CERSA477/10	95	129.8 ± 7.7 <sup>a</sup> ; 115.6 ± 10.1 <sup>b</sup>	2.00 ± 0.21 <sup>a</sup> ; 2.06 ± 0.21 <sup>b</sup>	64.7 ± 3.5	62.5% >2D <sub>0</sub> . Minimum age
VC34-2 Q <sup>1</sup>	CERSA477/11	99	88.4 ± 8.4 <sup>b</sup>	1.92 ± 0.19 <sup>b</sup>	48.0 ± 4.3	66.7% >2D <sub>0</sub> ; outlier, possible light contamination
VC34-3 Q <sup>1</sup>	CERSA477/12	105	114.5 ± 11.2 <sup>a</sup>	1.67 ± 0.17 <sup>a</sup>	68.8 ± 6.7	66.7% >2D <sub>0</sub> . Minimum age
VC34-4 Q <sup>1</sup>	CERSA477/31	231	87.3 ± 7.4 <sup>a</sup> ; 105.9 ± 12.0 <sup>b</sup>	1.82 ± 0.18 <sup>a</sup> ; 1.87 ± 0.19 <sup>a</sup>	57.9 ± 5.3	62.5% >2D <sub>0</sub> . Minimum age
VC34-5 Q <sup>1</sup>	CERSA477/32	234	107.4 ± 11.2 <sup>a</sup> ; 98.0 ± 9.5 <sup>b</sup>	1.43 ± 0.15 <sup>a</sup> ; 1.47 ± 0.15 <sup>b</sup>	68.9 ± 5.2	76.3% >2D <sub>0</sub> . Minimum age
VC34-6 Q <sup>1</sup>	CERSA477/33	237	96.0 ± 11.3 <sup>b</sup>	1.17 ± 0.12 <sup>b</sup>	81.9 ± 9.7	40.0% >2D <sub>0</sub> . Minimum age
VC34-7 Q <sup>1</sup>	CERSA477/36	259	73.8 ± 3.1 <sup>a</sup>	0.82 ± 0.11 <sup>a</sup>	89.6 ± 3.8	16.7% >2D <sub>0</sub>
VC34-8 Q <sup>1</sup>	CERSA477/37	264	68.8 ± 4.1 <sup>a</sup>	0.78 ± 0.11 <sup>a</sup>	88.7 ± 5.3	20.8% >2D <sub>0</sub>
VC35-1 Q <sup>2</sup>	NCL-3120121	65-80	103.3 ± 5.7	1.48 ± 0.06	69.9 ± 4.9	41% >2D <sub>0</sub> . Best estimate age
VC35-1 F <sup>2</sup>	NCL-3120121	65-80	161.7 ± 5.1	2.26 ± 0.16	76.4 ± 6.0	0% >2D <sub>0</sub>
VC35-2 Q <sup>2</sup>	NCL-3120122	150-165	110.6 ± 6.8	1.60 ± 0.07	69.0 ± 5.1	39% >2D <sub>0</sub> Best estimate age
VC35-2 F <sup>2</sup>	NCL-3120122	150-165	125.4 ± 5.1	2.39 ± 0.16	56.1 ± 4.5	0% >2D <sub>0</sub> . Outlier, reversal
VC35-3 Q <sup>2</sup>	NCL-3120123	283-290	62.9 ± 2.3	0.71 ± 0.04	88.0 ± 5.7	10% >2D <sub>0</sub>
VC35-3 F <sup>2</sup>	NCL-3120123	283-290	101.3 ± 4.2	1.50 ± 0.15	72.2 ± 8.0	3.4% >2D <sub>0</sub>
VC36-1 Q <sup>2</sup>	NCL-3120124	145-160	124.4 ± 5.8	1.51 ± 0.06	82.6 ± 5.2	39% >2D <sub>0</sub> . Best estimate age
VC36-1 F <sup>2</sup>	NCL-3120124	145-160	149.9 ± 5.0	2.29 ± 0.16	69.9 ± 5.5	0% >2D <sub>0</sub>

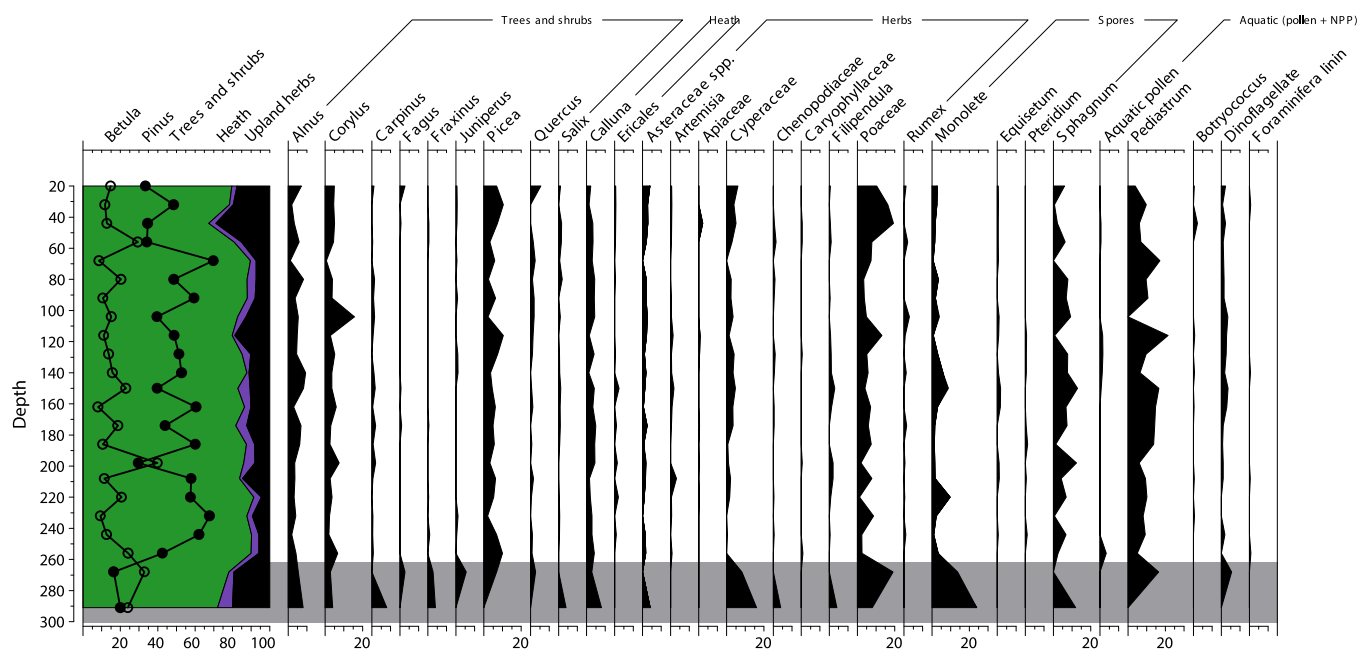


**Figure 5.** Percentage pollen diagram of core VC35, excluding species with only single occurrences. The lowest two samples, indicated with the grey band, have are almost barren and are therefore unreliable. [Color figure can be viewed at [wileyonlinelibrary.com](http://wileyonlinelibrary.com)]

## Discussion

The BB Fm is widespread in the southern North Sea, but a consistent interpretation of its age, facies and depositional environment was previously lacking. This inhibits confident age correlations and, consequently, broad-scale environmental reconstructions needed to understand the Late Pleistocene development of the southern North Sea basin. Our analysis of three vibrocores and 2D high-resolution acoustic reflection profiles at the flank of Het Gat (FG), east of the Brown Bank ridge, provides a

new framework on the stratigraphy, depositional age and depositional environment of the BB Fm at its type locality.

### Chronostratigraphic constraint

The new set of luminescence ages obtained for our study is a much-needed addition to a still limited set of chronostratigraphic controls for the BB Fm and its substrate, and thus for the Early Weichselian (MIS5d–a) of the region. Here we will

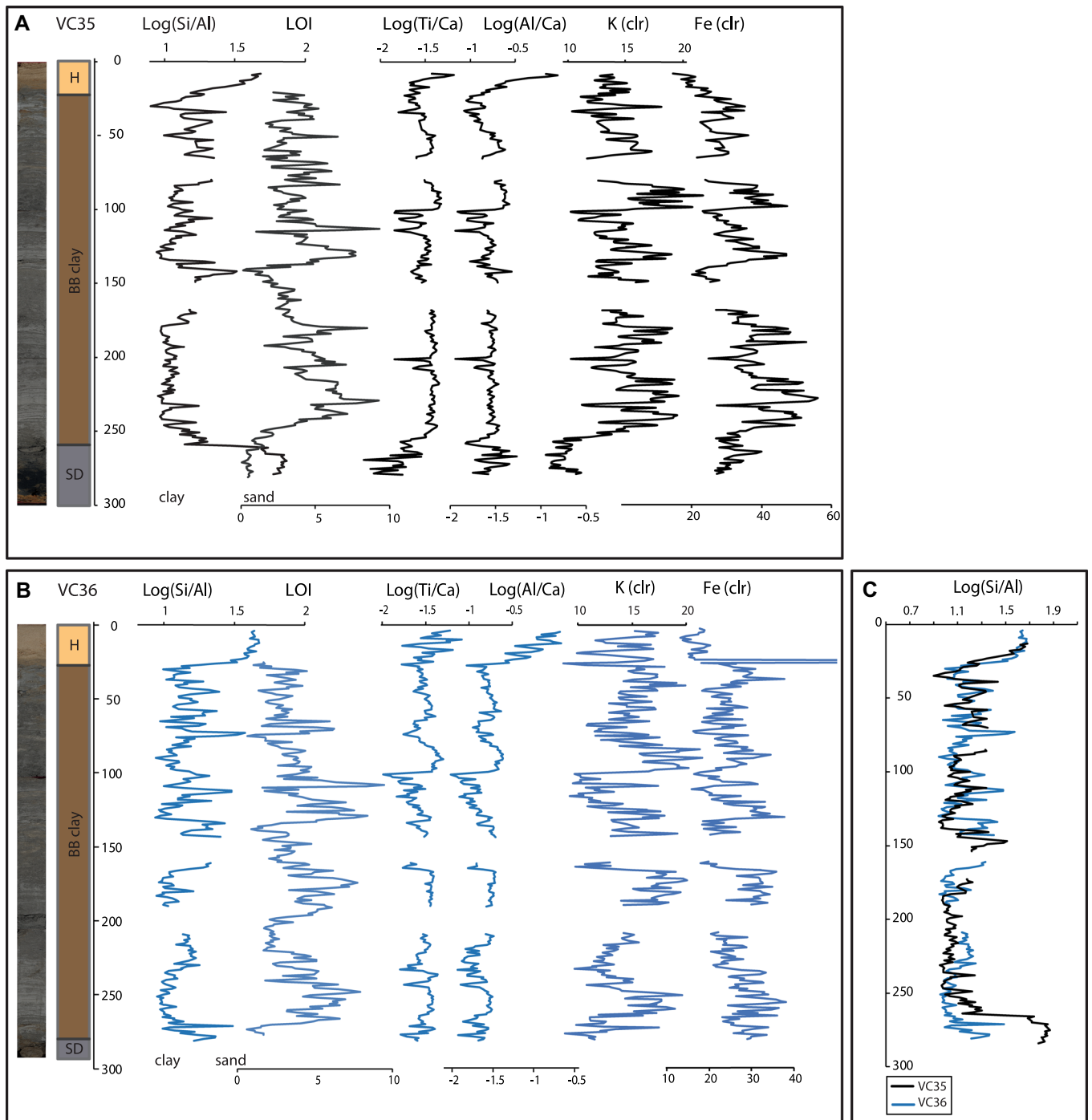


**Figure 6.** (A) XRF and LOI data for VC35; (B) XRF and LOI data for VC36; (C) comparison of  $\log(\text{Al}/\text{Si})$  of cores VC35 and VC36, where VC35 is shifted 5 cm down to align the top of the BB clay unit. Simplified sedimentary units are depicted on the left, with H = Holocene sand unit; BB clay = Brown Bank clay unit; SD = sand- dune unit. [Color figure can be viewed at [wileyonlinelibrary.com](https://onlinelibrary.com)]

apply the following correlation between terrestrial and marine stadial–interstadials of the Early Weichselian: MIS5d – Herning stadial, MIS5c – Brørup interstadial, MIS5b – Rederstall stadial, MIS5a – Odderade interstadial (Fig. 7) (e.g. Sánchez Goñi et al., 2005; Shackleton et al., 2002; Wohlfarth, 2013).

The top of the sand dune unit, dated at an average around 84–93 ka, can be linked to the temperate Odderade interstadial (MIS5a) and/or the Rederstall stadial (MIS5b) (Fig. 7). The more inconsistent quartz OSL ages of the BB clay unit yield an average age of 69–78 ka, but the most reliable samples from this set (i.e. VC34-6, VC35-2Q and VC36-1Q) suggest the older side of the age range is most reliable. The true age of the clay unit is underestimated by most clay-rich samples from the BB Fm, and the age of the BB clay unit probably ranges between 70 and

80 ka, which is indicative for deposition around the transition from the Odderade interstadial (MIS5a) into the Early Pleniglacial period (MIS4; Fig. 7). The good preservation of the dune morphology and draping of the clay layers above the dunes make a long hiatus between the dune deposition and the BB clay improbable, and favour the older age estimate.

The wide range of luminescence dates in the BB Fm can be narrowed down by pollen analysis of the clay unit. Abundant *Pinus* and low but clear presence of thermophilous trees indicate deposition during a temperate interstadial phase. Published pollen zones for the Netherlands and northwestern Germany show Early Weichselian (EW) stadials characterised by open vegetation with limited tree growth, and interstadials with the development of boreal coniferous forests (e.g. Behre, 1989; Kasse

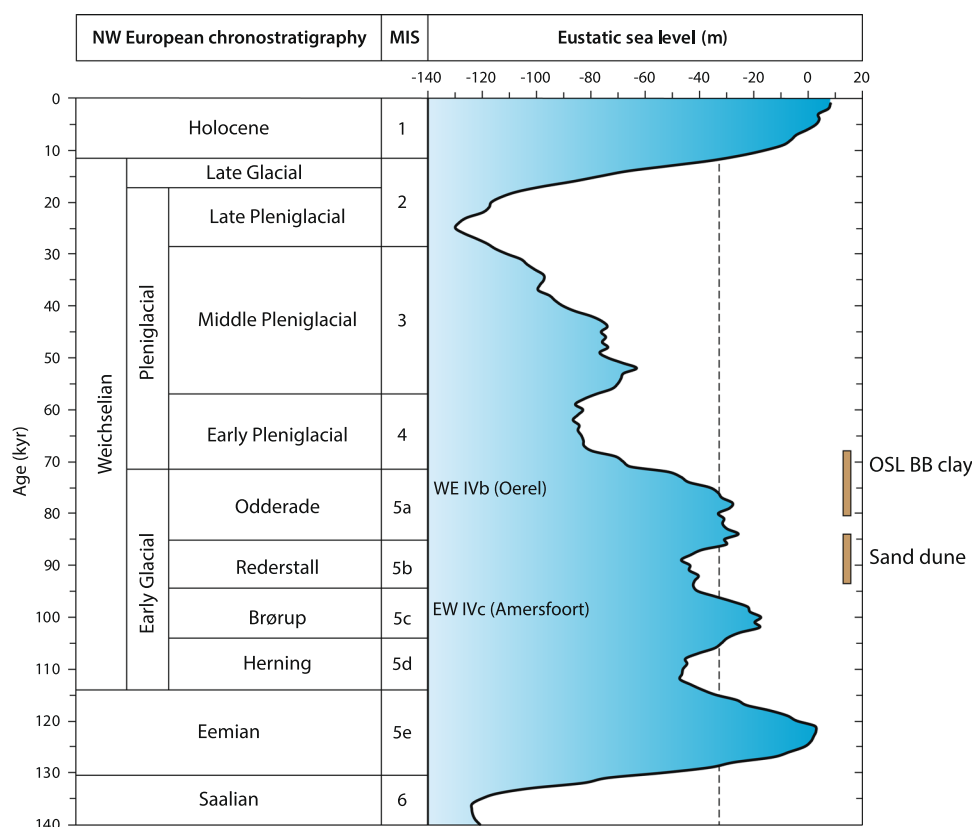


**Figure 7.** NW European chronostratigraphy, including marine isotope stages (MIS) and eustatic sea level (Spratt & Lisiecki, 2016). The ages of the chronostratigraphic stages, including those in the main text, are based on Lisiecki & Raymo (2005). The dashed line represents the reconstructed sea floor depth during deposition of  $-33$  m. The pollen zones EW IVc from the Amersfoort basin (Zagwijn, 1961) and zone EW IVb from Oerel (Behre, 1989) are indicated at the late Brörup and Odderade interstadial respectively. The OSL ages of the sand dune unit and the BB clay unit are both indicated on the right. [Color figure can be viewed at [wileyonlinelibrary.com](http://wileyonlinelibrary.com)]

et al., 2022; Zagwijn, 1961, 1983). Comparing our new data to the previously described pollen zones from the Amersfoort basin (Zagwijn, 1961) gives the best resemblance to zone EW IVc, which is the latest phase of the Brörup interstadial (MIS5c, ca. 96 ka). However, the records from the Amersfoort basin do not extend into younger parts of the Early Weichselian. The Oerel record in North Germany (Behre, 1989) provides a more complete record of the Early Weichselian. Our data are most comparable to pollen zones EW IIb (end of Brörup) and EW IVb (end of Odderade). EW IVb is most similar in the sum of trees, shrubs and herbs, while the presence of thermophilous trees (*Quercus*, *Carpinus*, *Corylus*) more resembles zone EW IIb. Based on pollen alone, it is clear that deposition occurred during the final phase of an Early Weichselian interstadial, but it is difficult to constrain if it was the end of the Brörup or Odderade interstadial. Comparing these pollen zones to the range of our OSL ages indicates that the BB Fm was deposited during the end of the Odderade interstadial (Fig. 7). After the Early Weichselian period, most of the Pleniglacial period had tundra, steppe or glacial desert landscapes in North-Western Europe (e.g. Sirocko et al., 2016). The pollen results are inconsistent with an Early Pleniglacial (MIS4) age for the BB clay sediments as suggested by some of the unreliable OSL results. Instead, the clay unit appears to be slightly older than most minimum OSL ages reported in Table 2; an age of 75–80 ka seems more plausible.

Our most reliable OSL ages are near the older limit of previous OSL ages reported for the BB Fm between 85 and 50 ka (Limpenny et al., 2011; Wessex Archaeology, 2018). Our pollen data differ from earlier pollen-based results of Zagwijn (1983), who concluded that deposition of the BB Fm started at the end of the Eemian and continued during the start of the Early Weichselian (MIS5d). It is still unclear if these differences are

systematic and have regional meaning, or if the BB Fm is more complex than previously assumed. The 2D high-resolution acoustic reflection profiles in Fig. 3 show the presence of a second, shallower and thus younger phase of the BB Fm east of the core location (BB2). It remains unknown if different parts of the BB Fm have formed in different time intervals during the Odderade interstadial only, or during subsequent interstadials.

As the BB Fm described in this location was deposited in a (restricted) marine setting, sea level must have been high enough to maintain marine conditions, which can provide an independent age indication. The water depth of the location is currently 39 m below MSL and the average Quaternary tectonic subsidence at the study location is approximately  $-0.085$  m  $\text{ka}^{-1}$  (Cohen et al., 2022). This results in an average background subsidence, without adjusting for glacio-isostasy, of about 6.4 m since the end of MIS5 (75 ka). Taking this background subsidence into consideration, the sea floor depth during deposition was around 33 m below MSL. During the peak of the Odderade interstadial (MIS5a) between 85 and 77 ka, global sea level was relatively high, around 25–35 m below MSL (Spratt & Lisiecki, 2016), which is probably represented by the sand dune facies (Fig. 7). After ca. 77 ka, minor global eustatic sea level fall started, and the BB clays were probably deposited at slightly lower sea levels in a more restricted setting. After ca. 74 ka, global sea level dropped below 40 m below MSL and therewith below the locality level (Gowan et al., 2021; Grant et al., 2014; Spratt & Lisiecki, 2016; Waelbroeck et al., 2002). During MIS3, the age interval suggested by some previously reported OSL results (Limpenny et al., 2011; Wessex Archaeology, 2018) as well as two outliers in our dataset, sea level remained too low to allow marine conditions at FG (Medina-Elizalde, 2013; Spratt &

Lisiecki, 2016). This would indicate an age for the sand dune unit of 85–77, and 77–74 for the BB clay unit. However, global eustatic sea level might have been different from local relative sea level in the southern North Sea, especially around the onset of MIS4, when ice sheets expanded rapidly and isostasy might have influenced local relative sea level. Combining the OSL ages, pollen stratigraphy and sea level constraints, we infer that the sand dune unit was deposited during the sea level highstand of MIS5a and the BB clay unit was deposited at the end of MIS5a. The deposits in this study thus provide the first detailed succession of the last interglacial–glacial transition (MIS5a–4 transition), a period of strong climate cooling, in the southern North Sea.

### *Depositional controls*

The sequence observed in our cores (area FG, Fig. 2) represents the infill of an elongated depression that probably formed by marine erosive process prior to or during deposition of an extensive overlying dune system. As we showed that the dunes were formed during early MIS5a, the depression could reflect early MIS5a sea-floor bathymetry although partial bathymetric relicts from older periods such as MIS5e and/or MIS5c cannot be excluded. This depression is overlain by a series of 1- to 2-m-high sand dunes. The asymmetrical cross-sectional nature of the dunes suggests they prograded northward, although more spatially distributed high-resolution acoustic reflection data are needed to confirm this. These sand dunes can be related to the sandy Lower Brown Bank unit described by Wessex Archaeology (2018), although having a younger age than previously described. Sand dunes within the BB Fm are present in the subsurface of British wind farm Norfolk Vanguard West (NVW; Eaton et al., 2020), ~60 km northwest of area FG. The dunes in their study are intercalated with finer-grained BB Fm sediment, whilst in the FG area they are directly on top of Middle Pleistocene strata. The dunes observed in NVW are also more symmetrical and have a wave period of only 40 m, an order of magnitude less than observed in this study. Although these sand dunes have different scales, which is no different from the modern sand dune field in the southern North Sea (Van der Meijden et al., 2023), it does indicate that this decrease in energy is common for the base of the BB Fm in the larger region. As the dunes described by Eaton et al. (2020) have not yet been dated and acoustic reflection correlations are still unavailable, it remains unknown whether both dune levels have the same stratigraphic position. This might either mean an initial fine-grained BB phase, contemporary with the sand dunes, is missing in our location, or that comparable dunes formed at different times and in somewhat differing settings throughout the southern North Sea area. In this latter instance, not all fine-grained facies would be part of the Upper Brown Bank unit as described by Wessex Archaeology (2018).

In the FG area the dunes are unconformably overlain by 2–4 m of organic-rich loams and silty clays, which relate to the Upper Brown Bank unit described by Wessex Archaeology (2018). In this area, two phases of the BB Fm are present (BB1 and BB2), but based on geophysical data (Fig. 3) alone it remained unclear if both units were present in the cores. As there is no distinct change in sedimentology, pollen content or elemental composition in the top of the BB clay unit, the cores only contain unit BB1, meaning that the stratigraphically higher, and thus younger, BB2 is missing in our analyses. Both the LOI and XRF analyses indicate higher terrestrial sediment input during deposition of the clay unit compared to the Holocene top layer, which suggests that the study area experienced a higher river input and/or a closer proximity of the coast at the MIS5a–4 transition compared to the modern situation. The variations in grain size may represent phases of fluctuating fluvial input to the site in the vicinity of the

Rhine–Meuse delta, which was also probably the primary source for these sediments (Hijma et al., 2012; Peeters et al., 2015).

The transition between the clays and underlying dune sands indicates that a pronounced change in depositional conditions occurred in the FG area towards the end of MIS5a. The well-preserved morphology of the sand dunes and the dominance of clay in the overlying sediments are typical of a transition from an open to a more restricted marine environment at the study site. Our observations are in agreement with a previously described low-energy depositional setting for the BB Fm, with clay overlying topographic irregularities (Cameron et al., 1989; Eaton et al., 2020). This generic transition thus does not seem to be forced locally, and might be related to delta-lobe avulsions, or even larger-scale drivers such as sea-level change or global climatic cooling during deposition.

Eaton et al. (2020) suggested that depositional conditions and bottom morphology during BB formation were controlled by changes in relative sea level. In their study area, only a few metres of sea-level lowering could have resulted in a change from a predominantly flooded shelf to a mostly subaerial landscape with enclosed and semi-enclosed lagoons. In their hypothesis, tidal processes were dominant during lower sea level, resulting in sand dune formation, whilst under high sea level lower-energy conditions were more conducive to deposition of fine-grained marine sediments. Although we agree with the suggested general sensitivity of this area to Early Weichselian sea-level variation, linking the sedimentary units to sea-level rise or fall is up for debate. Our new chronological data suggest that the clays were actually deposited during a phase when eustatic sea level was already lowering (late MIS5a), suggesting that the marine environment became more restricted and disconnected. In our alternative hypothesis, the submarine sand dunes were deposited under higher sea level and stronger tidal currents than the overlying BB Fm. During subsequent, or continued, sea-level fall at the end of MIS5a, the marine environment became more restricted and disconnected and most tidal currents were limited, resulting in fine-grained sediment deposition. Research on changing Holocene tidal conditions and tide-induced sand transport in the southern North Sea showed the strong influence of sea-level change to tidal currents (Van Der Molen & De Swart, 2001). Since the current near-highstand seafloor is indeed affected by tidal currents and covered in sand dunes and ripples, we consider this second hypothesis to be the most consistent with field observations. The ridges on the east and west side of the FG could have restricted currents within the FG area during low sea level, but even initial formation of larger compartments could have changed tidal flow.

### *Future directions*

At site FG, the BB Fm consists of an upper and lower Brown Bank unit, which represent decreasing energy in the North Sea water during late MIS5a, a temperate interstadial, towards the transition into MIS4, a cold stadial. The effect of climate change on the low-lying coastal landscape of the southern North Sea and its surroundings during this time period remains poorly understood, and a detailed study on the link between palaeoclimate and depositional setting from the cores described in this paper is ongoing. Furthermore, the geophysical survey data show the presence of a shallower phase of BB Fm (BB2, Fig. 3) east of the FG area. This indicates that besides the two phases of the BB Fm described in this paper, more phases, including younger phases, of Brown Bank deposition are present. The presence of these younger phases of the BB Fm implies that this part of the southern North Sea was, at least occasionally, submerged beyond 70–80 ka.

Recently collected geophysical survey data show evidence of even more depositional phases of the BB Fm. The subdivision into an Upper and Lower BB Fm thus seems to be a simplification of

the complex nature of this Formation. It remains unknown if these phases were dominated by delta-lobe avulsions, sea-level variations or other forcings. Future work to understand how many phases are represented in the BB Fm, and when they took place, should focus on regional patterns rather than local studies. Further analysis of the clastic and organic content, and of the observed grain-size variability in particular, will provide more information on the interacting and highly variable depositional environments involved in creating this marker horizon.

## Conclusion

The BB Fm is an easily recognisable and traceable seismostratigraphic unit present in large regions of the southern North Sea. The sedimentary succession on the east side of the Brown Bank Ridge has been studied to better understand the sedimentology, depositional setting and age of the BB Fm deposition. The sedimentology indicates a sudden decrease in energy in the depositional environment, accompanied by an increase in terrestrial and organic input. A combination of OSL dating, pollen biostratigraphy and global sea-level limits suggests that the BB Fm in this location was deposited during late MIS5a. These new results indicate that the sea floor of the southern North Sea remained submerged until at least late MIS5a. This new insight into the changing depositional setting at the interglacial–glacial transition raises the question of how climate change during this time interval influenced the marine landscape of the southern North Sea Basin.

**Acknowledgements.** We would like to thank the staff of the luminescence laboratories at the Netherlands Centre for Luminescence Dating and at the School of Earth and Environmental Sciences for their luminescence measurements. The authors appreciate the support of the ‘Europe’s Lost Frontier’ project, a European Research Council Advanced Grant at the Department of Archaeological and Forensic Sciences, University of Bradford (UK), and Martin Bates for providing core descriptions for VC34. We thank the Royal Netherlands Institute for Sea Research (NIOZ) and the Flanders Marine Institute (VLIZ), and the crews of RV Pelagia and RV Belgica for taking cores and acoustic data, Wim Hoek for laboratory assistance and Thomas Mestdagh for processing the MPES data.

## Data availability statement

The luminescence data that supports the findings of this study are available in the supplementary material of this article. Pollen, LOI and XRF data are available in the Neotoma Paleocology database (<https://www.neotomadb.org/>).

## Supporting information

Additional supporting information can be found in the online version of this article.

**Abbreviations.** BB Fm, Brown Bank Formation;  $D_0$ , parameter quantifying the ‘onset of saturation’;  $D_e$ , equivalent dose; EW, Early Weichselian; LOI, loss on ignition; MIS, marine isotope stage; MPES, multi-transducer parametric echosounder; MSL, mean sea level; NVW, Norfolk Vanguard West; OSL, optically stimulated luminescence; pIRIR, post-infrared infrared; SAR, single-aliquot regenerative dose; SD, Sand Dune unit; VC, vibrocore; XRF, X-ray fluorescence; YR, Yarmouth Roads.

## References

Aitchison, J. (1982) The statistical analysis of compositional data. *Journal of the Royal Statistical Society: Series B (Methodological)*,

- 44(2), 139–160. Available at: <https://doi.org/10.1111/j.2517-6161.1982.tb01195.x>
- Behre, K.E. (1989) Biostratigraphy of the last glacial period in Europe. *Quaternary Science Reviews*, 8(1), 25–44. Available at: [https://doi.org/10.1016/0277-3791\(89\)90019-X](https://doi.org/10.1016/0277-3791(89)90019-X)
- Bicket, A. & Tizzard, L. (2015) A review of the submerged prehistory and palaeolandscapes of the British Isles. *Proceedings of the Geologists’ Association*, 126(6), 643–663. Available at: <https://doi.org/10.1016/j.PGEOA.2015.08.009>
- Blanchet, C.L., Thouveny, N. & Vidal, L. (2009) Formation and preservation of greigite (Fe<sub>3</sub>S<sub>4</sub>) in sediments from the Santa Barbara Basin: implications for paleoenvironmental changes during the past 35 ka. *Paleoceanography*, 24(2), 1–15. Available at: <https://doi.org/10.1029/2008PA001719>
- Bos, I.J., Busschers, F.S. & Hoek, W.Z. (2012) Organic-facies determination: a key for understanding facies distribution in the basal peat layer of the Holocene Rhine–Meuse delta, The Netherlands. *Sedimentology*, 59(2), 676–703. Available at: <https://doi.org/10.1111/j.1365-3091.2011.01271.x>
- Cameron, T.D.J., Crosby, A., Balson, P.S., Jeffery, D.H., Lott, G.K., Bulat, J. et al. (1992) *United Kingdom offshore regional report: the Geology of the southern North Sea*. HMSO for the British Geological Survey
- Cameron, T.D.J., Laban, C. & Schüttenhelm, R.T.E. (1984) *Flemish Bight, Sheet 52°N-02°E, 1:250,000 series, Quaternary Geology*. British Geological Survey and Rijks Geologische Dienst
- Cameron, T.D.J., Schüttenhelm, R.T.E. & Laban, C. (1989) Middle and Upper Pleistocene and Holocene stratigraphy in the southern North Sea between 52° and 54°N, 2° to 4°E. In: Henriët, J.P. & De Moor, G. (Eds.) *The Quaternary and Tertiary Geology of the Southern Bight, North Sea*. Ministry of Economic Affairs – Belgian Geological Survey. pp. 119–136.
- Carlson, A.E., Stoner, J.S., Donnelly, J.P. & Hillaire-Marcel, C. (2008) Response of the southern Greenland Ice Sheet during the last two deglaciations. *Geology*, 36(5), 359–362. Available at: <https://doi.org/10.1130/G24519A.1>
- Cohen, K.M., Cartelle, V., Barnett, R., Busschers, F.S. & Barlow, N.L.M. (2022) Last Interglacial sea-level data points from Northwest Europe. *Earth System Science Data*, 14, 2895–2937. Available at: <https://doi.org/10.5194/essd-2021-390>
- Dean, W.E. (1974) Determination of carbonate and organic matter in calcareous sediments and sedimentary rocks by loss on ignition: comparison with other methods. *Journal of Sedimentary Petrology*, 44(1), 242–248. Available at: <https://doi.org/10.1306/74D729D2-2B21-11D7-8648000102C1865D>
- Eaton, S.J., Hodgson, D.M., Barlow, N.L.M., Mortimer, E.E.J. & Mellett, C.L. (2020) Palaeogeographical changes in response to glacial–interglacial cycles, as recorded in Middle and Late Pleistocene seismic stratigraphy, southern North Sea. *Journal of Quaternary Science*, 35(6), 760–775. Available at: <https://doi.org/10.1002/JQS.3230>
- EMODnet Bathymetry Consortium. (2020) European Marine Observation Data Network (EMODnet) Bathymetry. <https://emodnet.eu/bathymetry> [accessed december 2020]
- Galbraith, R.F., Roberts, R.G., Laslett, G.M., Yoshida, H. & Olley, J.M. (1999) Optical dating of single and multiple grains of quartz from Jinmium rock shelter, northern Australia: Part I, experimental design and statistical models. *Archaeometry*, 41(2), 339–364. Available at: <https://doi.org/10.1111/j.1475-4754.1999.tb00987.x>
- Gowan, E.J., Zhang, X., Khosravi, S., Rovere, A., Stocchi, P., Hughes, A.L.C. et al. (2021) A new global ice sheet reconstruction for the past 80000 years. *Nature Communications*, 12(1199), 1–9. Available at: <https://doi.org/10.1038/s41467-021-21469-w>
- Grant, K.M., Rohling, E.J., Ramsey, C.B., Cheng, H., Edwards, R.L., Florindo, F. et al. (2014) Sea-level variability over five glacial cycles. *Nature Communications*, 5(5076), 5076. Available at: <https://doi.org/10.1038/ncomms6076>
- Harff, J., Endler, R., Emelyanov, E., Kotov, S., Leipe, T., Moros, M. et al. (2011) Late Quaternary Climate Variations Reflected in Baltic Sea Sediments. In *The Balthic Sea Basin* (99–132). [https://doi.org/10.1007/978-3-642-17220-5\\_5](https://doi.org/10.1007/978-3-642-17220-5_5)
- Heiri, O., Lotter, A.F. & Lemcke, G. (2001) Loss on ignition as a method for estimating organic and carbonate content in sediments:

- reproducibility and comparability of results. *Journal of Paleolimnology*, 25(1), 101–110.
- Hijma, M.P., Cohen, K.M., Roebroeks, W., Westerhoff, W.E. & Busschers, F.S. (2012) Pleistocene Rhine–Thames landscapes: geological background for hominin occupation of the southern North Sea region. *Journal of Quaternary Science*, 27(1), 17–39. Available at: <https://doi.org/10.1002/JQS.1549>.
- Huntley, D.J. & Lamothe, M. (2001) Ubiquity of anomalous fading in K-feldspars and the measurement and correction for it in optical dating. *Canadian Journal of Earth Sciences*, 38(7), 1093–1106.
- Kasse, C., Van Der Woude, J.D., Woolderink, H.A.G. & Schokker, J. (2022) Eemian to Early Weichselian regional and local vegetation development and sedimentary and geomorphological controls, Amersfoort Basin, The Netherlands. *Netherlands Journal of Geosciences*, 101(e7), 1–22. Available at: <https://doi.org/10.1017/njg.2022.4>
- Laban, C. (1995) *The Pleistocene Glaciations in the Dutch Sector of the North Sea. A Synthesis of Sedimentary and Seismic Data*. [University of Amsterdam]. <https://hdl.handle.net/11245/1.119444>
- Limpenny, S.E., Barrio Froján, C., Cotterill, C., Foster-Smith, R.L., Pearce, B., Tizzard, L. et al. (2011) The East Coast Regional Environmental Characterisation. In *Cefas Open report 08/04, MEPP*.
- Lisiecki, L.E. & Raymo, M.E. (2005) A Pliocene–Pleistocene stack of 57 globally distributed benthic  $\delta^{18}\text{O}$  records. *Paleoceanography*, 20, PA1003.
- Martin-Puertas, C., Tjallingii, R., Bloemsmas, M. & Brauer, A. (2017) Varved sediment responses to early Holocene climate and environmental changes in Lake Meerfelder Maar (Germany) obtained from multivariate analyses of micro X-ray fluorescence core scanning data. *Journal of Quaternary Science*, 32(3), 427–436. Available at: <https://doi.org/10.1002/jqs.2935>
- Medina-Elizalde, M. (2013) A global compilation of coral sea-level benchmarks: implications and new challenges. *Earth and Planetary Science Letters*, 362, 310–318. Available at: <https://doi.org/10.1016/j.epsl.2012.12.001>
- Missiaen, T., Fitch, S., Harding, R., Muru, M., Fraser, A., De Clercq, M. et al. (2021) Targeting the Mesolithic: interdisciplinary approaches to archaeological prospection in the Brown Bank area, southern North Sea. *Quaternary International*, 584, 141–151. Available at: <https://doi.org/10.1016/j.QUAINT.2020.05.004>
- Mol, D., Post, K., Reumer, J.W.F., de Vos, J. & Laban, C. (2003) Het Gat: preliminary note on a Bavelian fauna from the North Sea with possibly two mammoth species. *Deinsea*, 9, 253–266.
- Murray, A., Arnold, L.J., Buylaert, J.P., Guérin, G., Qin, J., Singhvi, A.K. et al. (2021) Optically stimulated luminescence dating using quartz. *Nature Reviews Methods Primers*, 1(1), 72. Available at: <https://doi.org/10.1038/s43586-021-00068-5>
- Murray, A.S., Thomsen, K.J., Masuda, N., Buylaert, J.P. & Jain, M. (2012) Identifying well-bleached quartz using the different bleaching rates of quartz and feldspar luminescence signals. *Radiation Measurements*, 47(9), 688–695. Available at: <https://doi.org/10.1016/j.radmeas.2012.05.006>
- Oele, E. (1971) The Quaternary geology of the southern area of the Dutch part of the North Sea. *Geologie en Mijnbouw*, 50(3), 461–474.
- Peeters, J., Busschers, F.S. & Stouthamer, E. (2015) Fluvial evolution of the Rhine during the last interglacial–glacial cycle in the southern North Sea basin: a review and look forward. *Quaternary International*, 357, 176–188. Available at: <https://doi.org/10.1016/j.QUAINT.2014.03.024>
- Peeters, J., Busschers, F.S., Stouthamer, E., Bosch, J.H.A., Van den Berg, M.W., Wallinga, J. et al. (2016) Sedimentary architecture and chronostratigraphy of a late Quaternary incised-valley fill: a case study of the late Middle and Late Pleistocene Rhine system in the Netherlands. *Quaternary Science Reviews*, 131, 211–236. Available at: <https://doi.org/10.1016/j.QUASCIREV.2015.10.015>
- Reimann, T., Thomsen, K.J., Jain, M., Murray, A.S. & Frechen, M. (2012) Single-grain dating of young sediments using the pIRIR signal from feldspar. *Quaternary Geochronology*, 11, 28–41. Available at: <https://doi.org/10.1016/j.quageo.2012.04.016>
- Sánchez Goñi, M.F., Bard, E., Landais, A., Rossignol, L. & D'errico, F. (2013) Air–sea temperature decoupling in western Europe during the last interglacial–glacial transition. *Nature Geoscience*, 6(10), 837–841. Available at: <https://doi.org/10.1038/ngeo1924>
- Sánchez Goñi, M.F., Loutre, M.F., Crucifix, M., Peyron, O., Santos, L., Duprat, J. et al. (2005) Increasing vegetation and climate gradient in Western Europe over the Last Glacial Inception (122–110 ka): data-model comparison. *Earth and Planetary Science Letters*, 231(1–2), 111–130. Available at: <https://doi.org/10.1016/j.epsl.2004.12.010>
- Shackleton, N.J., Chapman, M., Sánchez-Goñi, M.F., Paillet, D. & Lancelot, Y. (2002) The Classic Marine Isotope Substage 5e. *Quaternary Research*, 58, 14–16. Available at: <https://doi.org/10.1006/qres.2001.2312>
- Sirocko, F., Knapp, H., Dreher, F., Förster, M.W., Albert, J., Brunck, H. et al. (2016) The ELSA-Vegetation-Stack: reconstruction of Landscape Evolution Zones (LEZ) from laminated Eifel maar sediments of the last 60,000 years. *Global and Planetary Change*, 142, 108–135. Available at: <https://doi.org/10.1016/j.gloplacha.2016.03.005>
- Spratt, R.M. & Lisiecki, L.E. (2016) A Late Pleistocene sea level stack. *Climate of the Past*, 12(4), 1079–1092. Available at: <https://doi.org/10.5194/cp-12-1079-2016>
- Tjallingii, R., Stattegger, K., Wetzel, A. & Van Phach, P. (2010) Infilling and flooding of the Mekong River incised valley during deglacial sea-level rise. *Quaternary Science Reviews*, 29(11–12), 1432–1444. Available at: <https://doi.org/10.1016/j.quascirev.2010.02.022>
- Van der Meijden, R., Damveld, J.H., Ecclestons, D.W., Van der Werf, J.J. & Roos, P.C. (2023) Shelf-wide analyses of sand wave migration using GIS: a case study on the Netherlands Continental Shelf. *Geomorphology*, 424, 108559. Available at: <https://doi.org/10.1016/j.geomorph.2022.108559>
- Van Der Molen, J. & De Swart, H.E. (2001) Holocene tidal conditions and tide-induced sand transport in the southern North Sea. *Journal of Geophysical Research: Oceans*, 106(C5), 9339–9362. Available at: <https://doi.org/10.1029/2000JC000488>
- Van Hoang, L., Clift, P.D., Schwab, A.M., Huuse, M., Nguyen, D.A. & Zhen, S. (2010) Large-scale erosional response of SE Asia to monsoon evolution reconstructed from sedimentary records of the Song Hong–Yinggehai and Qiongdongnan Basins, South China Sea. *Geological Society, London, Special Publications*, 342, 219–244. Available at: <https://doi.org/10.1144/SP342.13>
- Waelbroeck, C., Labeyrie, L., Michel, E., Duplessy, J.C., McManus, J.F., Lambeck, K. et al. (2002) Sea-level and deep water temperature changes derived from benthic foraminifera isotopic records. *Quaternary Science Reviews*, 21(1–3), 295–305. Available at: [https://doi.org/10.1016/S0277-3791\(01\)00101-9](https://doi.org/10.1016/S0277-3791(01)00101-9)
- Wallinga, J. & Cunningham, A.C. (2015) Luminescence Dating, Uncertainties, and Age Range. In: Rink, W. & Thompson, J., (Eds.) *Encyclopedia of Scientific Dating Methods*. Netherlands: Springer. pp. 440–445. In <https://doi.org/10.1007/978-94-007-6326-5>
- Weltje, G.J. & Tjallingii, R. (2008) Calibration of XRF core scanners for quantitative geochemical logging of sediment cores: theory and application. *Earth and Planetary Science Letters*, 274(3–4), 423–438. Available at: <https://doi.org/10.1016/j.epsl.2008.07.054>
- Wessex Archaeology. (2018) *Norfolk Vanguard Offshore Wind Farm Stage 3 Geoarchaeological Sampling and Assessment* (Issue March). <https://corporate.vattenfall.co.uk/globalassets/uk/projects/norfolk-vanguard/en010079-000022-scoping-report-6.pdf>
- Wintle, A.G. & Murray, A.S. (2006) A review of quartz optically stimulated luminescence characteristics and their relevance in single-aliquot regeneration dating protocols. *Radiation Measurements*, 41(4), 369–391. Available at: <https://doi.org/10.1016/j.RADMEAS.2005.11.001>
- Wohlfarth, B. (2013) A review of Early Weichselian climate (MIS 5d-a) in Europe. Technical report/Svensk kärnbränslehantering AB
- Zagwijn, W.H. (1961) Vegetation, climate and radiocarbon datings in the Late Pleistocene of the Netherlands. Part I: Eemian and Early Weichselian. *Mededelingen van de Geologische Stichting, Nieuwe Serie*, 14, 15–40.
- Zagwijn, W.H. (1983) Sea-level changes in the Netherlands during the Eemian. *Geologie en Mijnbouw*, 62, 437–450.